12th IFAC International Symposium on
Advanced Control of Chemical Processes
July 14-17, 2024. Toronto, Canada

Nonlinear Model Predictive Control of Hydrocyclone Separation Efficiency ⋆

Stefan Jespersen * **Dennis Severin Hansen** *
Mads Valentin Bram * **Mahsa Kashani** * **Zhenyu Yang** *

* *AAU Energy, Aalborg University, Esbjerg, Denmark (e-mail: sje@energy.aau.dk, dsh@energy.aau.dk, mvb@energy.aau.dk, maka@energy.aau.dk, yang@energy.aau.dk).*

Abstract: As oil fields mature, an increasing volume of water is produced alongside the oil and gas due to the injection of water to maintain reservoir pressure. The control of de-oiling hydrocyclones in produced water treatment on offshore oil and gas facilities is typically based on the pressure drop ratio (PDR). While PDR relates to the flow split in the hydrocyclone and affects the separation efficiency, it is only an indirect way to control the steady-state de-oiling efficiency. When the separation facility is subjected to disturbances, e.g., changing inlet concentration or production volume, the separation efficiency changes dynamically. The PDR responds to changes in flow rate, but it cannot sense changes in inlet oil content. By deploying online oil-in-water monitors, the separation efficiency could, in principle, be measured and used for dynamic feedback. This work developed a plant model based on previously published models of PDR, separator water level, and hydrocyclone separation efficiency. A nonlinear model predictive controller is designed and placed in cascade with the existing PDR-based PI controller to optimize the hydrocyclone separation efficiency. The results indicate an increased separation efficiency and, thus, a potential reduction in discharged oil of approximately 12 percentage points.

Keywords: De-oiling hydrocyclone, separation efficiency, nonlinear model predictive control, produced water treatment

1. INTRODUCTION

Although green energy production is increasing globally, oil and gas will remain a significant component of the global energy demand for decades. As the oil fields mature, water makes up an increasing proportion of the total produced volume, straining the produced water treatment (PWT) facility.

An offshore PWT facility often consists of three-phase separator tanks, where gas, oil, and water are separated based on their density difference. The oil skims over a weir plate into the oil compartment while the water is further treated downstream. De-oiling hydrocyclones are used extensively as the secondary treatment process in offshore treatment facilities before the remaining oil is discharged into the ocean or re-injected into the reservoir.

The produced water (PW) discharge is subject to regulations to reduce its impact on the marine environment. In the North Sea, the concentration limit of PW is currently 30 mg/L (approximately 30 ppm) based on a monthly average of manual samples. Installation of online oil-in-water (OiW) monitors is also required for reporting (Miløstyrelsen (2018)).

The coupled three-phase separators and hydrocyclones in PWT facilities are typically controlled using separate PID controllers, as seen in Fig. 1 (Husveg et al. (2007b); Yang et al. (2013)). The interface level between oil and gas in the three-phase separator is controlled by manipulating the underflow valve of the hydrocyclone, and the system is subjected to disturbances d_{Level}, such as changes in production rates, e.g., caused by slug flow (Sivertsen et al. (2010)).

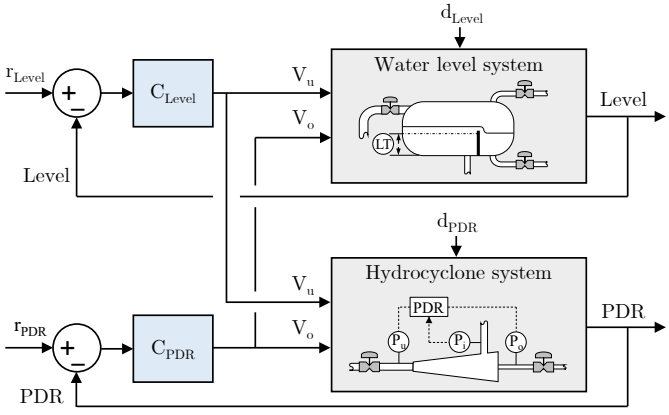

Fig. 1. Block diagram of the typical control of a PWT facility using separate PID controllers for the water level in the three-phase separator and the pressure drop ratio in the hydrocyclone system.

Conventional control relies on maintaining a fixed flow split defined as

⋆ The authors thank the support from the Danish Offshore Technology Centre (DOTC).

$$F_s = \frac{Q_o}{Q_i}, \tag{1}$$

where Q_i, Q_o, and Q_u are the inlet, overflow, and underflow flow rates, respectively. Typically, the overflow is much smaller than the underflow $Q_u \gg Q_o$, thus, the flow rate of the underflow is often considered as $Q_u \approx Q_i$. Instead of measuring F_s directly, the pressure drop ratio (PDR) is typically used as the controlled variable (CV) due to the approximate linear relationship between PDR and F_s as studied by Husveg et al. (2007b), where

$$PDR = \frac{P_i - P_o}{P_i - P_u}. \tag{2}$$

The P_i, P_o, and P_u are the pressures at the inlet, overflow, and underflow, respectively. This type of control strives to achieve a sufficient steady-state separation efficiency while reducing the amount of water exiting through the overflow (Husveg et al. (2007b)).

The hydrocyclone separation efficiency is often represented by the concentration-reducing efficiency given by

$$\varepsilon = 1 - \frac{C_u}{C_i}, \tag{3}$$

where C_i and C_u are the OiW concentrations at the inlet and underflow (discharge), respectively.

Much research has focused on improving PDR-based control since the de-oiling efficiency of the hydrocyclone is affected by changes in the feeding flow rate disturbing the PDR (d_{PDR}) Husveg et al. (2007b,a); Durdevic and Yang (2018b); Hansen et al. (2018). Some PDR-based multiple-input-multiple-output control solutions have been proposed in recent years, such as robust H_∞ control by Durdevic and Yang (2018b); Jespersen et al. (2021) and model predictive control by Hansen et al. (2018); Jespersen et al. (2021) where OiW monitors were used for performance evaluation.

OiW-based control has also been considered in recent years. In Vallabhan K.G. et al. (2020), a nonlinear first principles model was developed based on droplet trajectory analysis and the Bernoulli equation. A PI controller was then tuned using the Skogestad internal model control (SIMC) method to control the discharge concentration in simulation. In addition, Vallabhan et al. designed numerous control solutions for the discharge concentration, such as sliding mode control, feedback linearization (Vallabhan K.G. and Holden (2020)), feedforward, cascade PI, and nonlinear model predictive control (NMPC) (Vallabhan K.G. et al. (2021)). The authors also tested a feedforward and cascaded PI on an experimental setup (Vallabhan K.G. et al. (2022)). Common for these solutions is that they relied on controlling the discharge concentration to a fixed reference. However, when the discharge concentration fell below the reference, the controller actuated V_o to reach the reference, leading to a larger discharge than necessary.

While the model in Vallabhan K.G. et al. (2020) has proven capable of modeling the steady-state efficiency of hydrocyclones, the dynamics have not been validated. In Jespersen et al. (2023a,b), the authors identified Hammerstein-Wiener models of the dynamic separation efficiency, volumetric rate of oil discharge and discharge concentration based on online OiW measurements. The identification experiment emulated an offshore oil and gas platform subjected to production flow disturbances while the existing level and PDR controllers were active. A SIMC-tuned PI-controller was used to demonstrate that the discharge concentration could be controlled to a fixed reference. However, ideally, the system should achieve the best possible separation performance at any given time without negatively impacting production, which is not guaranteed by a fixed reference of discharge concentration.

In this work, a plant model is developed by combining existing models of the three-phase separator water level and PDR from Hansen et al. (2018) and Durdevic and Yang (2018a), and the separation efficiency model from Jespersen et al. (2021). A NMPC - that optimizes the separation efficiency of the hydrocyclone - is designed and placed in cascade with the existing PDR-based PI controller. The purpose of this idea is to add the OiW-based control as a layer on top of the existing PDR-based control, which, instead of a fixed flow split, optimizes the PDR reference to improve the separation efficiency with no negative effects on production.

The rest of the paper is organized as follows: Section 2 presents the combined plant model and model validation and the NMPC design, and Section 3 presents the simulation results. Section 4 discusses the results and methods, and Section 5 concludes the paper.

2. METHODS

2.1 System model

A diagram of the system considered in this study with the cascaded NMPC is given in Fig. 2. The plant model consists of a separator water level model, a model of the hydrocyclone PDR, and a model of the separation efficiency, as well as classical PI controllers of the level and PDR normally existing on a PWT facility. The inputs to the separator level model are the underflow valve opening degree V_u as the manipulated variable (MV) and the production flow rate Q_{in} as a disturbance input. The inputs to the PDR and efficiency model are the underflow and overflow valve opening degrees V_u and V_o, with V_o as MV and the hydrocyclone inlet concentration C_i as a disturbance.

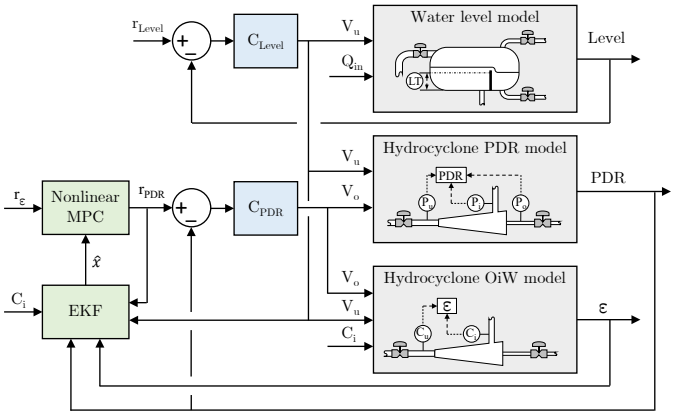

Fig. 2. Block diagram of the combined system model.

The *Water level model* block in Fig. 2 is a linear model of the water/oil interface level in the three-phase separator,

while the *Hydrocyclone PDR model* is a Hammerstein PDR model used in Hansen et al. (2018). The level and PDR dynamics are described by a state-space representation

$$\dot{\boldsymbol{x}} = \boldsymbol{A}\boldsymbol{x} + \boldsymbol{B}\boldsymbol{u} \tag{4a}$$
$$\boldsymbol{y} = \boldsymbol{C}\boldsymbol{x} + \boldsymbol{D}\boldsymbol{u}, \tag{4b}$$

where $\boldsymbol{A} \in \mathbb{R}^{5\times5}$, $\boldsymbol{B} \in \mathbb{R}^{5\times3}$, $\boldsymbol{C} \in \mathbb{R}^{2\times5}$, and $\boldsymbol{D} = \mathbf{0_{3,3}}$. The first state represents the evolution of the water level, while the states 2-5 are black-box states representing the evolution of PDR. The non-zero coefficients of the state-space model are given in Table 1.

Table 1. The coefficients of the state-space matrices for the level and PDR model in (4).

$\boldsymbol{A}$	$\boldsymbol{B}$	$\boldsymbol{C}$
$a_{11} = -1.2300{\cdot}10^{-5}$	$b_{11} = -1.3685{\cdot}10^{-3}$	$c_{11} = 1$
$a_{22} = -9.7445{\cdot}10^{-1}$	$b_{13} = 1.7000{\cdot}10^{-3}$	$c_{23} = 2.7204$
$a_{23} = -7.6063{\cdot}10^{-1}$	$b_{21} = -1$	$c_{25} = 1.6872$
$a_{32} = 1$	$b_{42} = 1$	
$a_{44} = -9.3155{\cdot}10^{-1}$		
$a_{45} = -6.5396{\cdot}10^{-1}$		
$a_{54} = 1$		

The inputs and outputs of the state-space model with the equilibrium point subtracted are

$$\boldsymbol{u} = \begin{bmatrix} u_{V_u} \\ u_{V_{o,h}} \\ Q_{in} \end{bmatrix} - \begin{bmatrix} 0.4168 \\ 0.1657 \\ 0.4 \end{bmatrix} \tag{5a}$$

$$\boldsymbol{y} = \begin{bmatrix} l \\ PDR \end{bmatrix} - \begin{bmatrix} 0.15 \\ 2 \end{bmatrix}, \tag{5b}$$

where Q_{in} is the production flow rate and $U_{V_{o,h}}$ is given by the Hammerstein function

$$u_{V_{o,h}} = \arctan(u_{V_o} k_1) k_2, \tag{6}$$

with $k_1 = 6$ and $k_2 = 0.2118$.

The level controller is given by

$$\frac{U_{V_u}(s)}{E_l(s)} = -58.37 - \frac{1.067}{s}, \tag{7}$$

and the PDR controller is given by

$$\frac{U_{V_o}(s)}{E_{PDR}(s)} = 0.1 + \frac{0.1}{s}. \tag{8}$$

These PI controllers were tuned in Durdevic and Yang (2018a) to represent the current offshore control solution.

In Fig. 2, the Hydrocylone OiW Model block consists of a black-box Hammerstein model of separation efficiency, by Jespersen et al. (2023a,b). This is a discrete-time Hammerstein model, which can be represented as

$$\boldsymbol{h}(k) = \boldsymbol{f_h}(\boldsymbol{u_\varepsilon}(k)) \tag{9a}$$
$$\boldsymbol{x_\varepsilon}(k+1) = \boldsymbol{A_\varepsilon}\boldsymbol{x_\varepsilon}(k) + \boldsymbol{B_\varepsilon}\boldsymbol{h}(k) \tag{9b}$$
$$y_\varepsilon(k) = \boldsymbol{C_\varepsilon}\boldsymbol{x_\varepsilon}(k) + \boldsymbol{D_\varepsilon}\boldsymbol{u_\varepsilon}(k), \tag{9c}$$

where $\boldsymbol{A_\varepsilon} \in \mathbb{R}^{7\times7}$, $\boldsymbol{B_\varepsilon} \in \mathbb{R}^{7\times3}$, $\boldsymbol{C_\varepsilon} \in \mathbb{R}^{1\times7}$ and $\boldsymbol{D_\varepsilon} = \mathbf{0_{3,3}}$. The coefficients of the state-space matrices are given in Table 2. The sampling time of the model is $T_s = 0.2$ s.

The input to the model $\boldsymbol{u_\varepsilon}$ with equilibrium values subtracted is

$$\boldsymbol{u_\varepsilon} = \begin{bmatrix} u_{V_u} \\ u_{V_o} \\ C_i \end{bmatrix} - \begin{bmatrix} 0.5053 \\ 0.6490 \\ 96.263 \end{bmatrix}, \tag{10}$$

The output y_ε in (9) is the ratio of concentrations in (3) and the separation efficiency in Fig. 2 is therefore given by

$$\varepsilon = 1 - (y_\varepsilon + 0.6237) = 0.3763 - y_\varepsilon. \tag{11}$$

Table 2. The coefficients of the state-space matrices for the efficiency model in (9).

$\boldsymbol{A_\varepsilon}$	$\boldsymbol{B_\varepsilon}$	$\boldsymbol{C_\varepsilon}$
$a_{11} = 1.9773$	$b_{11} = 1$	$c_{11} = 1$
$a_{12} = -9.7771{\cdot}10^{-1}$	$b_{32} = 1$	$c_{13} = 1$
$a_{21} = 1$	$b_{53} = 2$	$c_{15} = -5.0571{\cdot}10^{-1}$
$a_{33} = 1.9257$		$c_{16} = 5.0000{\cdot}10^{-1}$
$a_{34} = -9.2653{\cdot}10^{-1}$		
$a_{43} = 1$		
$a_{55} = 1.8884$		
$a_{56} = -1.0015$		
$a_{57} = 4.3143{\cdot}10^{-1}$		
$a_{65} = 1$		
$a_{76} = 2.5000{\cdot}10^{-1}$		

The Hammerstein function is comprised of three one-dimensional third-order polynomials, i.e., one for each input

$$f_{h,i}(u_i, \alpha_i) = \alpha_{i,0} + \alpha_{i,1}u_i + \alpha_{i,2}u_i^2 + \alpha_{i,3}u_i^3, \tag{12}$$

where i denotes the ith input. The polynomial coefficients are given in table 3.

Table 3. Polynomial coefficients in the Hammerstein part of the separation efficiency model.

	f_{h,V_u}	f_{h,V_o}	f_{h,C_i}
α_0:	$-4.4771{\cdot}10^{-5}$	$1.1890{\cdot}10^{-5}$	$3.2580{\cdot}10^{-2}$
α_1:	$1.7127{\cdot}10^{-4}$	$-7.1076{\cdot}10^{-5}$	$1.7473{\cdot}10^{-3}$
α_2:	$2.8924{\cdot}10^{-4}$	$5.5993{\cdot}10^{-4}$	$-3.7555{\cdot}10^{-5}$
α_3:	$-2.8959{\cdot}10^{-4}$	$4.1371{\cdot}10^{-4}$	$-1.8688{\cdot}10^{-6}$

2.2 Model Validation

For the validation of the model, experimental data is used from a lab-scaled pilot plant with the level and PDR control active, while the system is subjected to varying production flow rate Q_{in} emulating slugging flow into the three-phase separator tank. For more information about the testing facility, refer to Jespersen et al. (2023b).

In Fig. 3, the comparisons between the experimental data and the plant model for water level and the V_u are presented. The match between the measured water level and the model is good, except around $t = 750$ s, where the level data and the model deviate as V_u fully opens. The shape of V_u also resembles the data nicely, but the model seems to overestimate the effect of V_u.

Fig. 4 compares the data and plant model for separation efficiency, PDR, and V_o. The fit to the separation efficiency is reasonable, except for the deviation around $t = 750$ s. At this period, the PDR model also has its largest deviation. The oscillations seen in the data are due to the chattering of V_o when V_u is almost closed. Except for these variations, the model captures most of the dynamics.

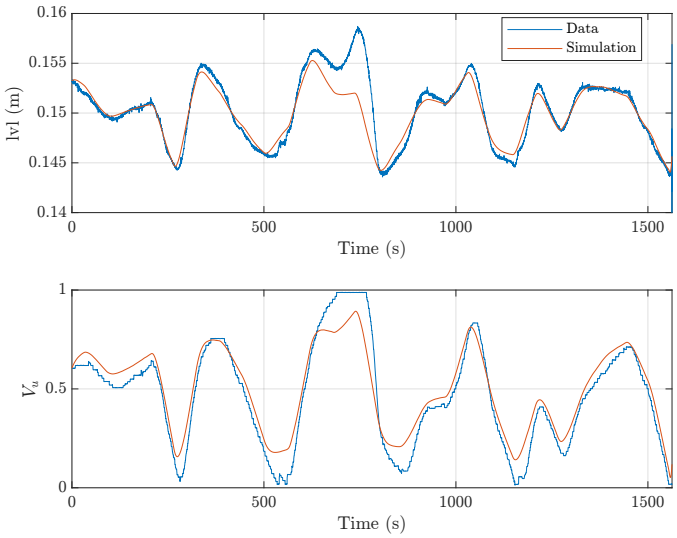

Fig. 3. Comparison between experimental data and the model for the water level (top) and the underflow valve opening degree V_u (bottom).

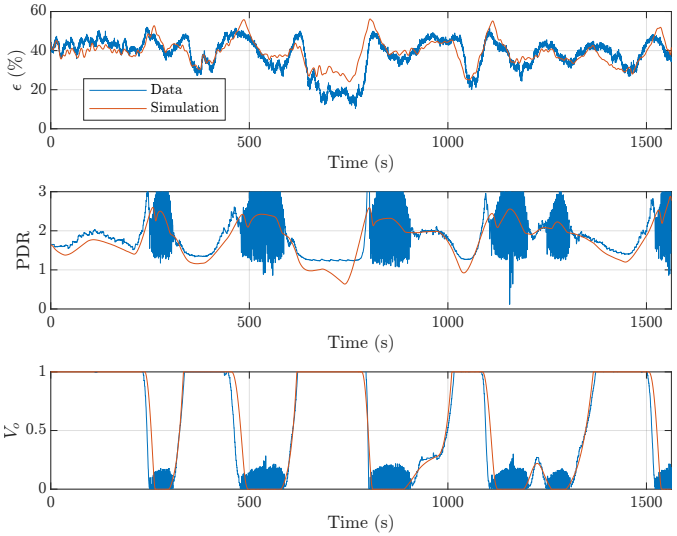

Fig. 4. Comparison between experimental data and the model for the hydrocyclone separation efficiency (top), the PDR (middle), and the overflow valve opening degree V_o (bottom).

2.3 Nonlinear Model Predictive Control

The NMPC extends the existing PDR control structure as a cascaded control solution with the PDR controller in the inner loop and the MPC in the outer loop. The resulting MPC is a single-input-single-output controller with the PDR reference as the MV and the separation efficiency as the CV. The prediction model inputs are the commanded underflow valve opening V_u, the measured hydrocyclone inlet concentration C_i, and the PDR reference.

For NMPC, a prediction model of the following form is needed

$$\boldsymbol{x}(k+1) = \boldsymbol{f}(\boldsymbol{x}(k), \boldsymbol{u}(k)) \tag{13}$$
$$\boldsymbol{y}(k) = \boldsymbol{h}(\boldsymbol{x}(k), \boldsymbol{u}(k)). \tag{14}$$

The prediction model is the *Hydrocyclone PDR model* with the PDR controller C_{PDR} and the *Hydrocyclone OiW model* in Fig. 2.

The continuous-time PDR model and the PDR controller are converted to discrete-time with sampling time $T_s = 0.2$ s. The states of the separation efficiency model remain unchanged as the model is already discrete.

The general objective of the hydrocyclone is to operate with maximum separation efficiency with as little water entering the overflow as possible (high de-watering efficiency). To achieve this, a multiobjective optimization problem could be posed with the simultaneous maximization of separation efficiency and minimization of flow split. As PDR is correlated with F_s, this could be posed as the minimization of the cost function

$$J(k) = \sum_{i=1}^{H_p} \left(-w_1 \hat{y}_\varepsilon(k+i|k)^2 - \frac{w_2}{\hat{y}_{PDR}(k+i|k)^2} \right), \tag{15}$$

where $\hat{y}_\varepsilon$ and $\hat{y}_{PDR}$ are the model predictions of separation efficiency and PDR while w_1 and w_2 are suitable weights. In this work, the weights $w_1 = 1$ and $w_2 = 0$ are chosen as a direct optimization of separation efficiency. The optimization problem is solved using the sequential quadratic programming method.

The prediction horizon was increased until insignificant improvements were seen, resulting in $H_p = 40$ samples, which corresponds to 8 s. The control horizon was selected as $H_c = 0.25 H_p$ corresponding to 2 s.

The prediction model must know the system state at the kth time step. An extended Kalman filter (EKF) estimates the system state based on measurements of the PDR and separation efficiency, as illustrated in Fig. 2. The EKF assumes additive Gaussian noise features. The measurement covariance is

$$\boldsymbol{R} = \begin{bmatrix} \sigma_\varepsilon^2 & 0 \\ 0 & \sigma_{PDR}^2, \end{bmatrix} \tag{16}$$

with $\sigma_\varepsilon = 0.0234$ and $\sigma_{PDR} = 0.0835$ determined from measurements. The process noise variance $\boldsymbol{Q} \in \mathbb{R}^{12\times12}$ where only non-zero element is assumed to be $q_{10,10} = 2.9533$, corresponding to the measurement noise of C_i. The initial state covariance is assumed to be small, i.e., $P_{0|0} = 0.001$.

3. RESULTS

The simulation experiment is a scenario with varying production rate Q_{in} and the resulting varying inlet concentration to the hydrocyclone C_i, as seen in Fig. 5. The hydrocyclone inlet concentration would generally be a function of the inlet flow rate to the hydrocyclone Q_i, and effectively V_u as it governs the residence time of the separator. In principle, C_i could be modeled, but filtered data from the testing facility subjected to the same inlet flow disturbance is used instead.

The level controller is kept identical in both simulations, and the level and V_u are therefore identical in Fig. 6. Because the level controller is strict, the level only varies about 0.01 m around the reference of 0.15 m, causing significant variations in V_u.

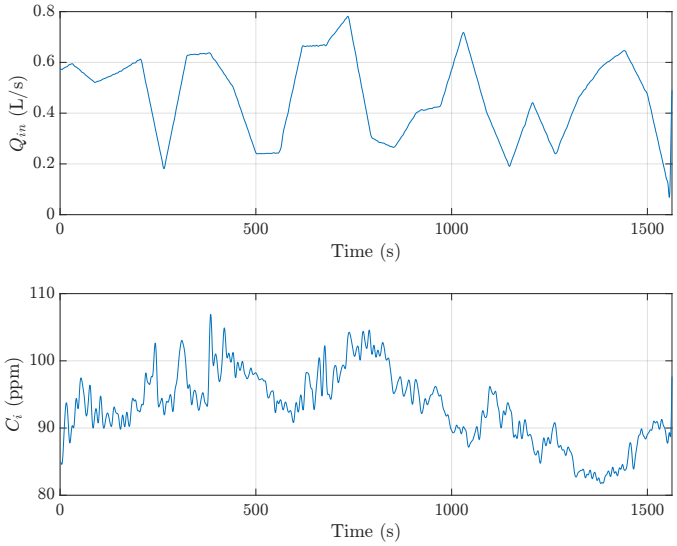

Fig. 5. The inlet flow to the separator tank Q_{in} and the resulting inlet oil concentration C_i to the hydrocyclone. The inputs are filtered data from the real process.

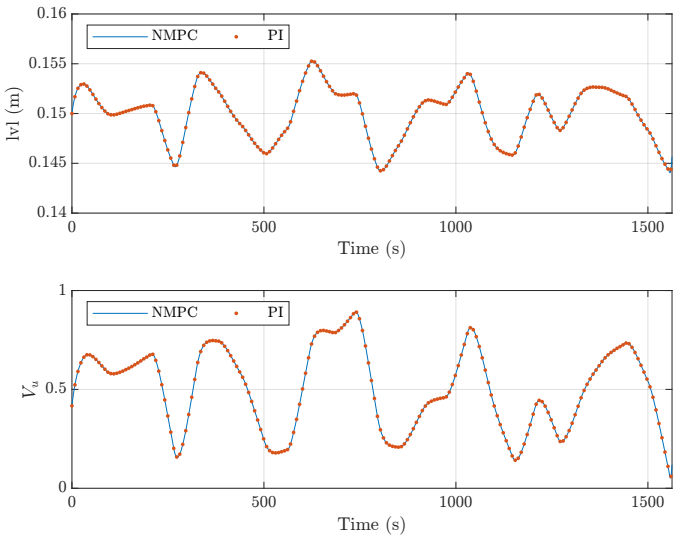

Fig. 6. The separator water/oil interface level and underflow valve (V_u) opening degree. The level controller gives the same response in both simulations.

In Fig. 7, the separation efficiency of the NMPC is higher than the PI controller alone over the whole simulation. The PI controller saturates V_o either fully open or fully closed, attempting to maintain PDR at the fixed reference of 2. The NMPC lets the PDR vary and only makes minor adjustments to V_o to keep it around the optimum value.

In Table 4, the mean and variance of the separation efficiency and the total valve travel of V_o are given. The NMPC achieved a mean separation efficiency of 50.77%, which is 11.7 percentage points (p.p.) better than the PI controller. The standard deviation of the separation efficiency achieved by the NMPC is also 1.85 p.p. larger than the efficiency of the PI controller. The overflow valve travel with the PI controller was 10.32 times the full valve travel, while with the NMPC it was only 0.45, corresponding to a reduction of 95.6% and thus effectively reduced valve wear.

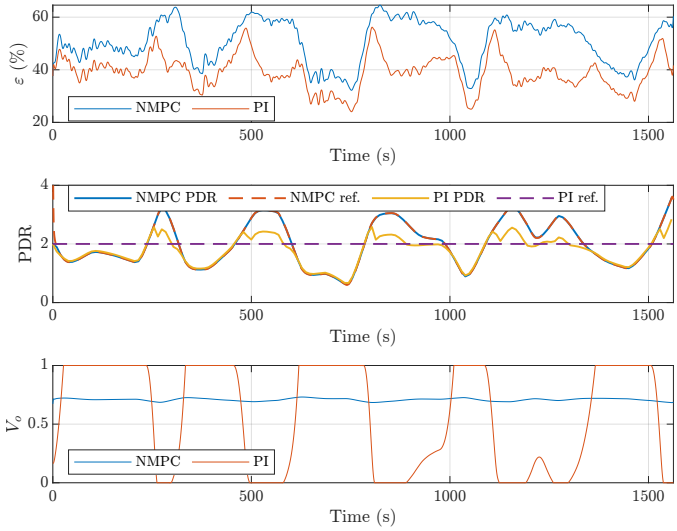

Fig. 7. The separation efficiency ε (top), the PDR and PDR references (middle), and the overflow valve opening degree V_o (bottom).

Table 4. Mean and standard deviation of separation efficiency and total overflow valve travel.

Performance metrics		Unit	NMPC	PID
Efficiency	mean	(%)	50.78	39.09
	SD	(%)	8.29	6.44
Total overflow valve travel		(-)	0.45	10.32

4. DISCUSSION

The addition of the NMPC improved the separation efficiency by 11.7 p.p. and reduced overflow valve actuation by 95.6%. While this represents a significant performance improvement, it is subject to some system assumptions. While the physical plant is interdependent, where almost every process change in one sub-system affects the rest of the system, this work has implemented simplifications. The model of the interface level is based on a mass balance using the orifice equation of the underflow valve. Typically, the overflow flow rate is only a couple of percent of the inlet flow rate, and the effect of V_o on the level is therefore neglected, as illustrated in Fig. 2. The level model is linearized around 0.15 m and a valve opening degree of $V_u = 0.4$ and assumes a constant pressure drop across the valve. The PDR model is linear in V_u and uses a Hammerstein black-box model to represent the effect of V_o with the equilibrium point of $PDR = 2$, $V_u = 0.4$, $V_o = 0.1657$, and $Q_{in} = 0.4$. The separation efficiency model is a nonlinear model identified on data from the process with the level and PDR controllers active. Therefore, the identification data only covered a subset of the possible valve combinations. In general, such black-box models may be less accurate when extrapolating outside the estimation data, but the model was deemed reasonable over most of the MV space (Jespersen et al. (2021)). Although the plant model used here may not perfectly describe the actual system, the PDR and level models have been successfully used to design advanced controllers (Hansen et al. (2018); Durdevic and Yang (2018a)), and the combined model captures most of the dynamics as seen in Fig. 4 and 3. Due to these model simplifications, the actual increase

in separation efficiency will likely be lower. Additionally, as seen in Fig. 7, the difference between the separation efficiency of the PI controller and the NMPC is largest when V_u is fully open, which causes the PI controller to open V_o completely. When V_o is fully open, the model reports a reduced separation efficiency, which is not typically observed. This may be due to the identification experiment discussed in Jespersen et al. (2021). Most authors report that the separation efficiency reaches a plateau in the overflow direction. This would reduce the improvement in separation efficiency additionally. However, in the North Sea, operators discharged approximately 4000 tonnes of oil between 2009 and 2019 (OSPAR (2022)). Thus, even minor improvements in separation efficiency can lead to significant reductions in produced water discharge.

5. CONCLUSION

In this work, a NMPC was designed to control the separation efficiency of a de-oiling hydrocyclone in a scaled version of a PWT facility. The NMPC is added on top of the existing PDR controller, and the comparison with and without the NMPC indicates significant improvements in separation efficiency and reduced valve wear. Due to the model simplifications and the scaled size of the testing facility, improvements on an offshore facility will likely be smaller. Still, the results show promising potential for OiW-based control of PWT systems.

Future works will include the separation efficiency of the three-phase separator to optimize the efficiency of the combined system to reduce the PW discharge even further.

ACKNOWLEDGEMENTS

The authors would like to thank project partners John Bagterp Jørgensen (DTU compute), Simon Ivar Andersen (DOTC), Ole Andersen (DOTC), and Benaiah Anabaraonye (DOTC). Thanks to AAU colleagues Simon Pedersen and Petar Durdevic for valuable discussions and technical support.

REFERENCES

Durdevic, P. and Yang, Z. (2018a). Application of H_∞ Robust Control on a Scaled Offshore Oil and Gas De-Oiling Facility. *Energies*, 11(2), 287. doi:10.3390/en11020287.

Durdevic, P. and Yang, Z. (2018b). Dynamic Efficiency Analysis of an Off-Shore Hydrocyclone System, Subjected to a Conventional PID- and Robust-Control-Solution. *Energies*, 11(9), 1–14. doi:10.3390/en11092379.

Hansen, L., Durdevic, P., Jepsen, K.L., and Yang, Z. (2018). Plant-wide Optimal Control of an Offshore De-oiling Process Using MPC Technique. *IFAC-PapersOnLine*, 51(8), 144–150. doi:10.1016/j.ifacol.2018.06.369. 3rd IFAC Workshop on Automatic Control in Offshore Oil and Gas Production OOGP 2018.

Husveg, T., Johansen, O., and Bilstad, T. (2007a). Operational Control of Hydrocyclones During Variable Produced Water Flow Rates—Frøy Case Study. *SPE Production & Operations*, 22(3), 294–300. doi:10.2118/100666-PA.

Husveg, T., Rambeau, O., Drengstig, T., and Bilstad, T. (2007b). Performance of a deoiling hydrocyclone during variable flow rates. *Minerals Engineering*, 20(4), 368–379. doi:10.1016/j.mineng.2006.12.002.

Jespersen, S., Hansen, D.S., Yang, Z., and Andersen, S.I. (2021). Flow-Loop Testing of Online Oil-in-Water UV-Fluorescence-Based Measurement. In *2021 IEEE 2nd International Conference on Signal, Control and Communication (SCC)*, 313–319. IEEE. doi:10.1109/SCC53769.2021.9768363.

Jespersen, S., Kashani, M., and Yang, Z. (2023a). Hammerstein-Wiener Model Identification Of De-Oiling Hydrocyclone Separation Efficiency. In *2023 9th International Conference on Control, Decision and Information Technologies (CoDIT)*, 2508–2513. IEEE. doi:10.1109/CoDIT58514.2023.10284508.

Jespersen, S., Yang, Z., Hansen, D.S., Kashani, M., and Huang, B. (2023b). Hammerstein–Wiener Model Identification for Oil-in-Water Separation Dynamics in a De-Oiling Hydrocyclone System. *Energies*, 16(20), 7095. doi:10.3390/en16207095.

Miløstyrelsen (2018). Generel tilladelse for Total E&P Danmark A/S (TOTAL) til anvendelse, udledning og anden bortskaffelse af stoffer og materialer, herunder olie og kemikalier i produktions- og injektionsvand fra produktionsenhederne Halfdan, Dan, Tyra og Gorm for perioden 1. januar 2019 - 31. december 2020. Technical report, Total E&P Danmark A/S, Copenhagen.

OSPAR (2022). Assessment of the impacts of the offshore oil and gas industry on the marine environment. Technical report, OSPAR.

Sivertsen, H., Storkaas, E., and Skogestad, S. (2010). Small-scale experiments on stabilizing riser slug flow. *Chemical Engineering Research and Design*, 88(2), 213–228. doi:10.1016/j.cherd.2009.08.007.

Vallabhan K.G., M. and Holden, C. (2020). Nonlinear control algorithms for de-oiling hydrocyclones. In *2020 28th Mediterranean Conference on Control and Automation (MED)*, Mediterranean Conference on Control and Automation, 85–90. IEEE. doi:10.1109/MED48518.2020.9183115.

Vallabhan K.G., M., Holden, C., and Skogestad, S. (2020). A First-Principles Approach for Control-Oriented Modeling of De-oiling Hydrocyclones. *Industrial and Engineering Chemistry Research*, 59(42), 18937–18950. doi:10.1021/acs.iecr.0c02859.

Vallabhan K.G., M., Holden, C., and Skogestad, S. (2022). Deoiling Hydrocyclones: An Experimental Study of Novel Control Schemes. *SPE Production & Operations*, 37(3), 462–474. doi:10.2118/209576-PA.

Vallabhan K.G., M., Matias, J., and Holden, C. (2021). Feedforward, Cascade and Model Predictive Control Algorithms for De-Oiling Hydrocyclones: Simulation Study. *Modeling, Identification and Control*, 42(4), 185–195. doi:10.4173/MIC.2021.4.4.

Yang, Z., Stigkær, J.P., and Løhndorf, B. (2013). Plant-wide Control for Better De-oiling of Produced Water in Offshore Oil & Gas Production. *IFAC Proceedings Volumes*, 46(20), 45–50. doi:10.3182/20130902-3-CN-3020.00143.